Acta Crystallographica Section D
Biological Crystallography
ISSN 1399-0047

Nitrate in the active site of protein tyrosine phosphatase 1B is a putative mimetic of the transition state

Peter W. Kenny, Janet Newman and Thomas S. Peat*

CSIRO Materials, Science and Engineering, 343 Royal Parade, Parkville, VIC 3052, Australia

Correspondence e-mail: tom.peat@csiro.au

Received 10 July 2013
Accepted 12 November 2013

PDB reference: protein tyrosine phosphatase 1B, 4bjo

The X-ray crystal structure of the complex of protein tyrosine phosphatase 1B with nitrate anion has been determined and modelled quantum-mechanically. Two protomers were present in the structure, one with the mechanistically important WPD loop closed and the other with this loop open. Nitrate was observed bound to each protomer, making close contacts with the S atom of the catalytic cysteine and a tyrosine residue from a crystallographically related protomer.

1. Introduction

Reversible phosphorylation of tyrosine residues is a common mechanism for regulating biochemical processes, and dephosphorylation is catalyzed by protein tyrosine phosphatases (PTPs). Protein tyrosine phosphatase 1B (PTP1B) is the prototypical member of this enzyme class and has been of particular interest to the pharmaceutical industry as a potential target for the treatment of both type 2 diabetes and obesity (Elchebly *et al.*, 1999; Zhang & Zhang, 2007; Combs, 2010). The many crystal structures of complexes of PTP1B reveal a deep, narrow binding site in which a number of electrostatic interactions between protein and ligand are shielded from solvent by closure of the WPD loop (Puius *et al.*, 1997; Asante-Appiah *et al.*, 2002; Liu *et al.*, 2003; Scapin *et al.*, 2003; Xin *et al.*, 2003; Lau *et al.*, 2004; Black *et al.*, 2005; Ala, Gonneville, Hillman, Becker-Pasha, Wei *et al.*, 2006; Ala, Gonneville, Hillman, Becker-Pasha, Yue *et al.*, 2006; Han *et al.*, 2008). Despite these attractive characteristics of its binding site, PTP1B has proved to be a relatively intractable target (Zhang & Zhang, 2007), in part reflecting the lack of useful bioisosteric replacements for the anionic portion of the proposed transition states. This difficulty in mimicking phosphoryl groups, especially when dianionic, may be a factor favouring the natural selection of reversible phosphorylation as a signalling mechanism (Black *et al.*, 2005).

PTP-catalyzed dephosphorylation takes place in two steps, the first of which is nucleophilic attack on phosphorus by the thiolate sulfur of the catalytic cysteine (Fig. 1). Crystal structures have been determined for the intermediate (Pannifer *et al.*, 1998) formed in this first step and the complex (Brandão *et al.*, 2010) with orthovanadate, which mimics the trigonal bipyramidal transition state. An earlier structure of the complex of PTP1B with orthovandate has also been reported (Peters *et al.*, 2003), although coordinates were not deposited in the Protein Data Bank (PDB; Bernstein *et al.*, 1977). The nitrate anion has been shown crystallographically (Fauman *et al.*, 1996) to mimic the equatorial portion of orthovanadate when bound to *Yersinia* PTP. This structure is of particular interest because the interactions between nitrate anion and

the protein are all noncovalent. It can be argued that the lack of covalent bonds between protein and ligand mean that the structure provides a more direct view of the stabilization of the transition state by the enzyme than would the structure of a covalently bound ligand.

In this study we have determined the crystal structure of PTP1B bound to nitrate, capturing the WPD loop in both the open and the closed forms. Fortuitously, a tyrosine residue from an adjoining (crystallographically related) molecule is found positioned in the active site, with the nitrate and tyrosine mimicking the transition state of the dephosphorylation reaction of phosphotyrosine by PTP1B. We have also used quantum-mechanical calculations to explore the interactions between nitrate anion and PTP1B, especially the unusually close contact with the cysteine thiolate anion. We compare these structures with those previously determined as transition-state analogues.

2. Materials and methods

2.1. Protein details

The sequence of human PTP1B was synthesized by DNA2.0 (Menlo Park, USA); the gene was excised from the cloning vector into a derivative of the pET43 expression vector using the enzymes *Bam*HI and *Nhe*I, and *Escherichia coli* BL21 (DE3) cells were transformed with this new expression plasmid. The construct contains an N-terminal His tag, a TEV protease site and the PTP1B sequence. Protein production was induced by addition of 0.5 m*M* IPTG at mid-log phase and the cells were then placed at 301 K and allowed to grow for a further 3 h before being spun down and the cell pellets stored at 193 K. Cells were lysed in an Avestin C5 cell homogenizer at 103 MPa with three passes and the sample was then clarified by centrifugation at 20 000 rev min^{-1} for 20 min at 277 K. The lysis buffer was buffer *A* (300 m*M* NaCl, 50 m*M* Tris pH 8.0, 10 m*M* imidazole, 5 m*M* DTT, 10% glycerol) plus a Roche cOmplete EDTA-free protease-inhibitor tablet, 0.5 mg ml^{-1} lysozyme, 2 m*M* $MgCl_2$ and Benzonase, 90 ml which was added to 19 g of cells for homogenization. After centrifugation, the cell supernatant was passed over a 1.0 ml HiTrap FF IMAC column previously equilibrated in buffer *A*. This was washed with ten column volumes of buffer *A* plus 10 m*M* imidazole and the protein was then eluted with a step gradient of buffer *A* plus 240 m*M* imidazole. Peaks from the IMAC column were further purified by size-exclusion chromatography (S200 16/60 column) in 150 m*M* NaCl, 50 m*M* Tris pH 8.0, 5 m*M* DTT.

The protein was concentrated to about 10 mg ml^{-1} and set up in crystallization trials of 300 nl protein solution plus 300 nl crystallant equilibrated at either 281 or 293 K against a reservoir consisting of 50 µl of the crystallant. All experiments were set up with a Phoenix crystallization robot (ARI, USA) in SD-2 plates (Molecular Dimensions, UK). Over 10 000 trials were set up, varying the crystallant and testing variations of the protein (cleaved *versus* uncleaved, co-crystals with putative binders *etc.*). The most reliable crystallization conditions contained either HEPES or Tris buffer at around pH 8, a mid-weight polyethylene glycol (PEG) between 20 and 30%(*w*/*v*) and a magnesium salt between 0.1 and 0.3 *M*. The PEGs that proved useful in crystallization included PEG 3350, PEG 4000, PEG MME 5000, PEG 6000 and PEG 8000. Various anions were tested for the magnesium salt: acetate, chloride, formate and nitrate. The protein crystal that yielded the best diffraction was obtained at 281 K using 100 m*M* HEPES pH 8.1, 25.4% PEG 4000, 225 m*M* $Mg(NO_3)_2$. Wells with microseeds gave initial crystals within 3 d, whereas experiments without microseeds did not show crystals until after about 14 d.

Crystals were taken to the MX-1 beamline of the Australian Synchrotron and were cryocooled directly in a nitrogen stream at 100 K. A complete data set was obtained by taking 360 1° oscillation, 2 s shots at an energy of 12 000 eV. The data were indexed using *XDS* (Kabsch, 2010) and scaled using *SCALA* (Winn *et al.*, 2011). Molecular replacement was performed with *Phaser* (McCoy *et al.*, 2007) using PDB entry 3a5j (N. Iwamoto, S. Ito, D. Sumi, M. Kobayashi & T. Kumagai, unpublished work) as a starting model. The model was

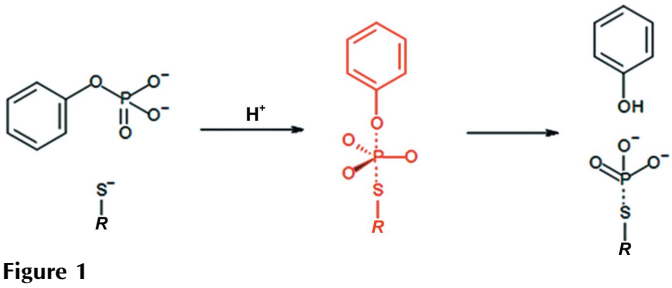

Figure 1
The first step of the catalytic reaction consists of a nucleophilic attack of the Cys215 thiolate on the P atom of the phosphotyrosine substrate that proceeds through a trigonal bipyramidal transition state, the equatorial portion of which is mimicked by nitrate anion. Addition of a proton facilitates departure of the tyrosine leaving group.

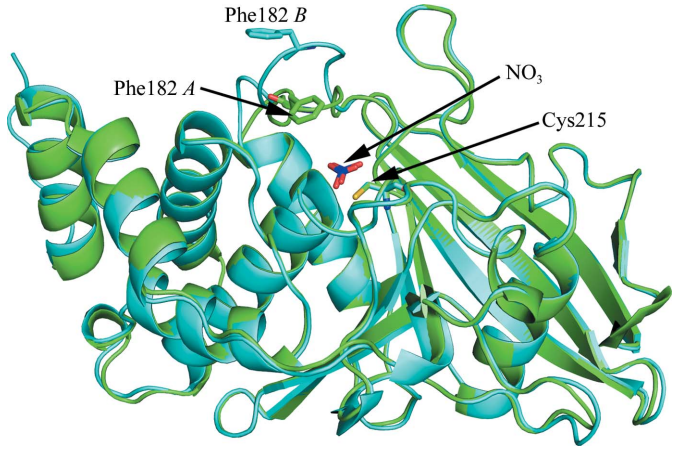

Figure 2
A superposition of protomer *B* on protomer *A* of the crystallographic structure. This figure shows the overall fold of PTP1B, the active-site cleft (highlighting the active-site cysteine) and the different positions that the WPD loop adopts in the two protomers. Rotation of protomer *B* onto protomer *A* using the *SSM* algorithm in *Coot* gives a r.m.s.d. of 0.6 Å, aligning 278 of the residues (out of 285/286).

manually rebuilt using *Coot* (Emsley *et al.*, 2010) and refined using *REFMAC* (Murshudov *et al.*, 2011). The overall fold of PTP1B showing the active site and the different positions of the WPD loops between protomer *A* and protomer *B* is shown in Fig. 2. Other than Fig. 1, which was produced with *Symyx Draw* (v.3.2), all figures were produced with *PyMOL* (DeLano Scientific, USA). The structure coordinates and structure factors have been deposited in the PDB (Bernstein *et al.*, 1977) as entry 4bjo. Data-collection and refinement statistics are given in Table 1.

2.2. Computational details

The complex of PTP1B with nitrate was modelled quantum-mechanically with the Hartree–Fock theoretical model (Szabo & Ostlund, 1996) and the 6-31G* basis set (Szabo & Ostlund, 1996) using the *Gaussian* 03 software (Frisch *et al.*, 2009). The protein was represented (Fig. 3) by portions of the residues making hydrogen-bonding contact with the nitrate anion, the Cys215 S atom or, in the case of the *A* protomer binding site, the water molecule observed 3.5 Å from the N atom of the nitrate anion. H atoms were added according to normal valency rules and molecular geometry was energy-minimized with non-H atom coordinates of the protein constrained to their crystallographic values. Both the Cys215 S atom and nitrate were modelled as anionic and the total charges of the *A* protomer site model, which included the cationic side chain of Arg221, and the *B* protomer site model were −1 and −2, respectively. Molecular electrostatic potential (MEP) stationary points (Fig. 4) were located for nitrate anion at the HF/6-31G* level using molecular geometry that had been energy-minimized at this level of theory and the *Gaussian* 03 keywords Prop = (EFG,Opt). Six equivalent MEP minima (−0.285 atomic units) were located in the plane defined by the atomic nuclei, and two equivalent saddle points (−0.178 atomic units) were found on the normal to this plane passing through the nucleus of the N atom.

3. Results

A comparison of the structures of the complexes of PTP1B (PDB entry 4bjo) and *Yersinia* PTP (PDB entry 1ytn; Fauman *et al.*, 1996) with nitrate shows that the *Yersinia* structure resembles the closed form (protomer *A*) of the PTP1B

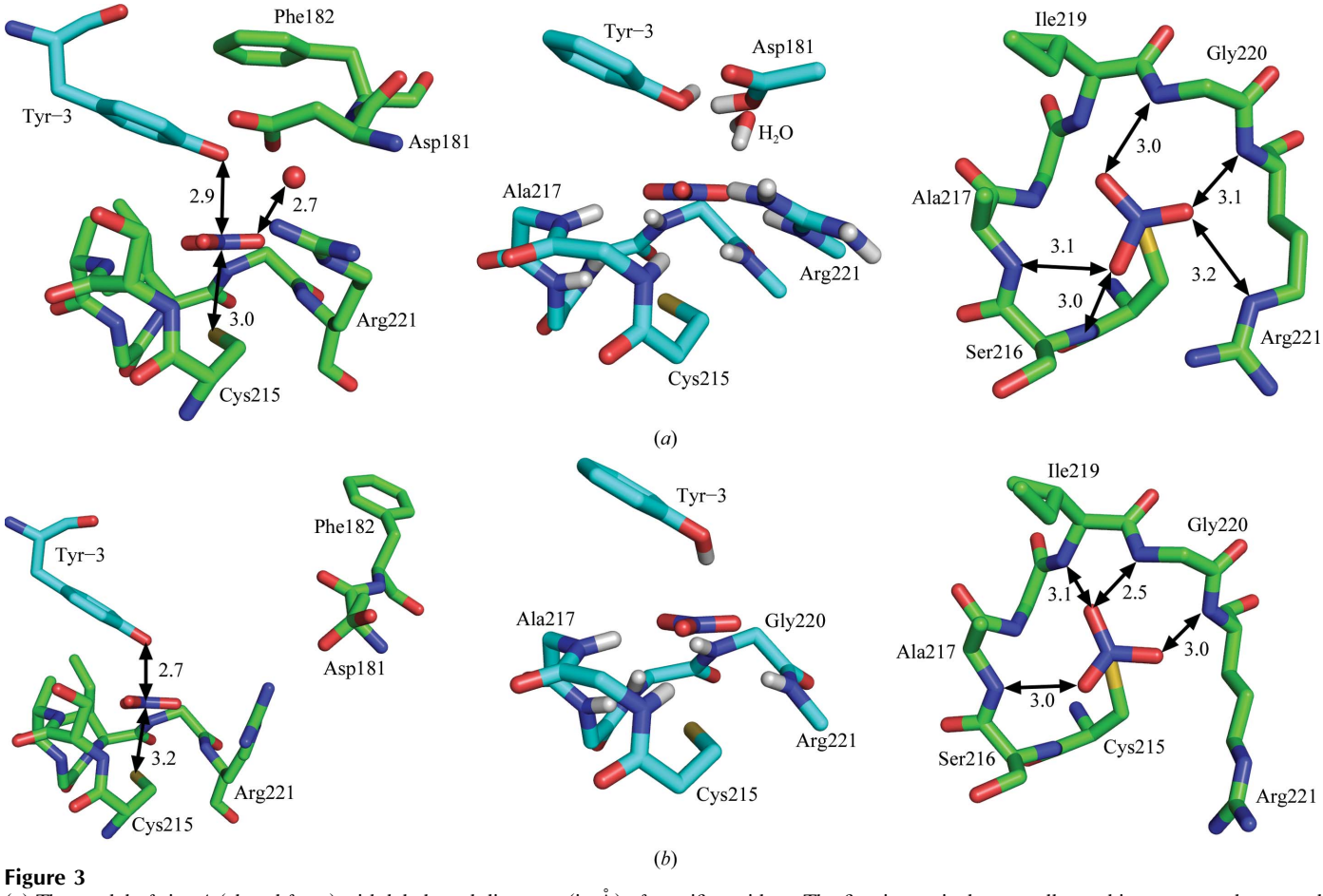

Figure 3
(*a*) The model of site *A* (closed form) with labels and distances (in Å) of specific residues. The first image is the crystallographic structure, the second image is of the quantum-mechanical model in the same orientation and the third image is the crystallographic structure at approximately 90° rotation (along the horizontal plane). (*b*) The model of site *B* (open form). It can be seen that in the open form both the WPD loop (Asp181 and Phe182 are shown here) are sitting outside the active site and that Arg221 moves and rotates its side chain out of hydrogen-bonding distance. The nitrate also shifts, moving towards Gly220 and up towards the tyrosine residue.

structure (Fig. 5). The two structures superpose reasonably well, with an r.m.s.d. of about 2 Å (1.9 Å for the *A* protomer and 2.3 Å for the *B* protomer) over 210 aligned residues (of ∼285) using the *SSM* algorithm in *Coot* (Emsley *et al.*, 2010). Although the nitrate sits in approximately the same space, there are differences in the nature of the contact with the inorganic anion. In the PTP1B structure, a crystallographically related protomer donates a tyrosine (Tyr−3, from the TEV protease site of the N-terminal His tag) that sits above the nitrate ion. The distance to the side-chain hydroxyl is 2.9 Å in the closed form (protomer *A*) and 2.7 Å in the open form (protomer *B*). This contact between tyrosine and nitrate means that the nitrate N atom is pentacoordinate, so this PTP1B structure provides a more complete model of the trigonal bipyramidal transition state than the structures of the *Yersinia* PTP nitrate complex or the orthovanadate complexes which lack the contact with tyrosine. As such, the binding of nitrate to the closed and open conformations of PTP1B can be described as two previously uncharacterized points on the

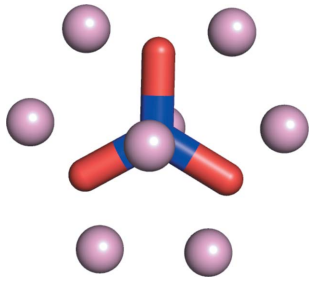

Figure 4
Energy-minimized structure of nitrate anion showing the locations of the MEP stationary points. The six points in the plane of the anion are minima and the two points on a normal to this plane passing through the nitrogen nuclear position are saddle points.

Table 1
Data-collection and refinement statistics.

PDB code	4bjo
Space group	*C*2
Unit-cell parameters (Å, °)	a = 161.6, b = 66.8, c = 68.8, β = 95.0
Data statistics	
Resolution limits (Å)	80.5–2.06 (2.17–2.06)
R_{merge}†	0.051 (0.609)
R_{meas}†	0.055 (0.689)
$R_{p.i.m.}$†	0.020 (0.311)
Total No. of observations	320288 (28222)
Total No. of unique observations	44854 (6139)
$\langle I/\sigma(I)\rangle$	23.6 (2.6)
$CC_{1/2}$‡	1.000 (0.858)
Completeness (%)	99.0 (93.5)
Average multiplicity	7.1 (4.6)
Refinement statistics	
R_{work}†	0.217
R_{free}†	0.239
Completeness (%)	98.9
R_{free} test set (%)	5.1
Average B value (Å^2)	49.9
Wilson B (Å^2)	43.9
No. of non-H atoms refined	4862
No. of waters	128
No. of metal/ligand atoms	18
R.m.s.d.§, bond distances (Å)	0.01
R.m.s.d.§, bond angles (°)	1.3
Ramachandran plot¶	
Favoured region (%)	96.5
Allowed region (%)	2.7
Outliers (%)	0.4
MolProbity analysis¶	
Poor rotamers	3 [0.6%]
Clashscore¶	1.91 [100th percentile]

† $R_{merge} = \sum_{hkl}\sum_i |I_i(hkl) - \langle I(hkl)\rangle|/\sum_{hkl}\sum_i I_i(hkl)$; $R_{meas} = \sum_{hkl}\{N(hkl)/[N(hkl)-1]\}^{1/2}\sum_i |I_i(hkl) - \langle I(hkl)\rangle|/\sum_{hkl}\sum_i I_i(hkl)$; $R_{p.i.m.} = \sum_{hkl}\{1/[N(hkl)-1]\}^{1/2}\sum_i |I_i(hkl) - \langle I(hkl)\rangle|/\sum_{hkl}\sum_i I_i(hkl)$; $R_{work} = \sum_{hkl}||F_{obs}| - |F_{calc}||/\sum_{hkl}|F_{obs}|$ and is calculated using all data; R_{free} is the R factor based on 5% of the data excluded from refinement. ‡ The use of $CC_{1/2}$ as reported for crystallography (Karplus & Diederichs, 2012). § R.m.s.d. is the root-mean-square deviation from ideal values (Engh & Huber, 1991). ¶ As determined by *MolProbity* (Chen *et al.*, 2010).

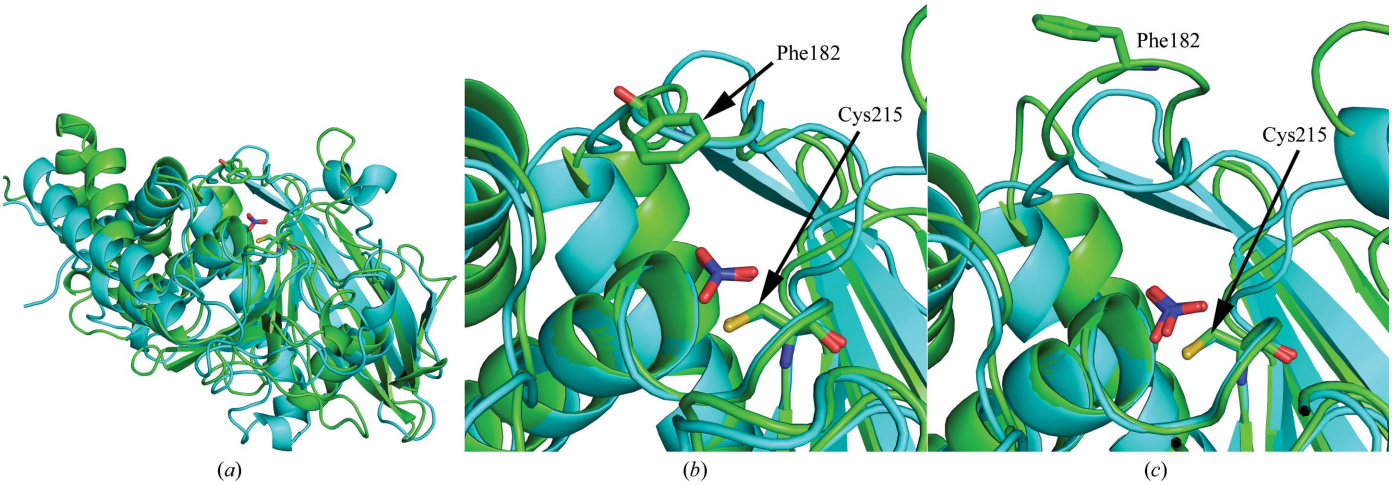

Figure 5
Superposition of *Yersinia* PTP with nitrate (PDB entry 1ytn) and the structures presented here of PTP1B with nitrate bound. (*a*) shows the *A* protomer superposed with PDB entry 1ytn. The sequence identity between PTP1B and the *Yersinia* PTP is about 18% and the superposition of C^α atoms gives an r.m.s.d. between the structures of 1.9 or 2.3 Å for the *A* and *B* protomers, respectively (using *SSM* in *Coot*). Further refinement (*LSQ* in *Coot*) of just active-site residues to the overall alignment gives a further movement of ∼0.3 Å (0.34 or 0.31 Å) and these alignments are shown in this figure. (*b*) and (*c*) are enlargements of the active site showing the nitrate as it is positioned over the active-site cysteine (Cys215 for PTP1B). Also highlighted is Phe182 in the WPD loop, showing how the *Yersinia* structure has this loop in the closed structure, similar to the *A* protomer (*b*) and unlike the *B* protomer in the open conformation (*c*).

reaction pathway. This tyrosine residue is sandwiched between Phe182 of the WPD loop (distances of 3.5–3.8 Å) and the nitrate in the closed form, but is relatively free to move in the open form (Figs. 3 and 6). The nitrate itself is held in place by multiple hydrogen bonds to backbone N atoms lining the active site of the protein. In the closed form the distances to the nitrate O atoms are N–Ser216 = 3.0 Å, N–Ala217 = 3.1 Å, N–Gly220 = 3.0 Å and N–Arg221 = 3.1 Å (there is also a water modelled in the active site of the closed form and this water is 2.7 Å from a nitrate O atom). In the open form, the distances to these O atoms are N–Ala217 = 3.0 Å, N–Ile219 = 3.1 Å, N–Gly220 = 2.5 Å and N–Arg221 = 3.0 Å. Thus, there is a slight movement from one side of the active site to the other side between the two independent protomers in the asymmetric unit. It is also interesting that in the open form the nitrate moves towards Tyr−3 and slightly away from Cys215 when compared with the closed form of the enzyme. One can see a subtle bulge of electron density towards the Cys215 S atom from the nitrate in the closed form (Fig. 6).

The quantum-mechanically modelled complexes were consistent with the crystal structures (Fig. 3). The distance observed between the nitrate N atom and cysteine sulfur for the *B* protomer (3.2 Å) is in close agreement with that found in the energy-minimized structure (3.1 Å). The nitrogen–sulfur distance modelled for the *A* protomer (3.3 Å) is less than 0.3 Å greater than its crystallographic equivalent, although this should not be considered surprising since modelling noncovalently bound complexes quantum-mechanically is considered to be a difficult problem (Grimme *et al.*, 2007). The location of minimum-energy geometries with anionic entities in such close proximity in both the *A* and *B* protomers is consistent with hydrogen-bond donation to both nitrate and Cys215 thiolate countering the electrostatic repulsion between these anionic entities.

4. Discussion

The binding modes observed for nitrate in this complex with PTP1B are particularly relevant to the catalytic mechanism of PTPs. Different conformations are observed for the WPD loop in the two protomers. Movement of the WPD loop is integral to the catalytic mechanism (Whittier *et al.*, 2013) and

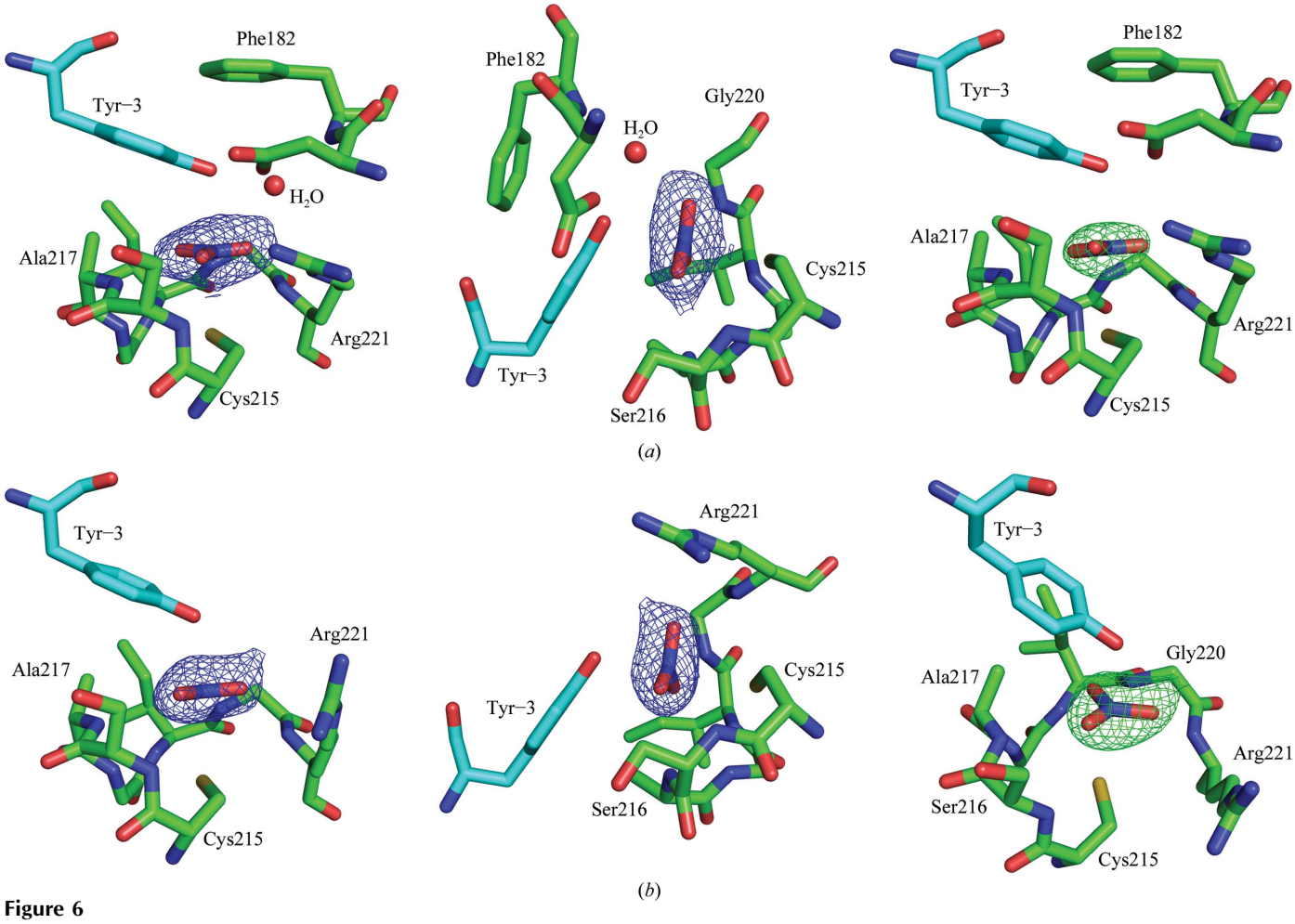

Figure 6
The electron density observed for the nitrate moiety and the residues of PTP1B protomers involved in binding the nitrate. (*a*) shows the closed form (protomer *A*) with $2mF_o - DF_c$ density at 1σ (0.21 e Å^{-3}) in the right and middle images (blue mesh); the images are rotated approximately 90° to each other. The rightmost image is similar in orientation to that of the first image, but shows an $mF_o - DF_c$ difference map at 3σ (0.11 e Å^{-3}; green mesh) of the nitrate after the nitrate was taken out of the model and the model was refined without the nitrate moieties. (*b*) shows similar images for the open form (protomer *B*).

we do not believe that both open and closed forms have been observed previously within a single crystal structure. It is unlikely that the open form (protomer *B*) is a consequence of crystal contacts, as the closest and only contact is from the Phe182 residue to a crystallographically related molecule at residues Asp240/Pro241, with no obvious hydrogen bonds or stacking interactions. The first step of the catalytic mechanism is the formation of a cysteinyl phosphate intermediate, and nitrate is a mimic for the equatorial portion of the trigonal bipyramidal transition state. This step can be thought of as a flow of negative charge from the (anionic) Cys215 to the O atoms of phosphotyrosine, and the enzyme functions by stabilizing this charge. Although crystal structures of a number of covalently bound transition-state analogues have been determined (Pannifer *et al.*, 1998; Brandão *et al.*, 2010), the complexes with nitrate (Fauman *et al.*, 1996) are of special interest because the anion is held in place by noncovalent interactions (Figs. 3 and 6). The nitrate anion is observed to hydrogen bond to Arg221 (the distance from Arg221 N^{ε} to the nitrate O atom is 3.2 Å) in the *A* protomer of the PTP1B structure, as it does in its complex with *Yersinia* PTP, and this might be expected to be the dominant charge-stabilizing interaction. However, the WPD loop is open in the *B* protomer and the absence of this interaction (the distance to Arg221 N^{ε} is 4.4 Å) presents a challenge to this assumption of dominance. To some extent, the *B* protomer can be seen as representing a missing link in the sequence (Pannifer *et al.*, 1998; Brandão *et al.*, 2010) of crystallographic snapshots of the catalytic mechanism, in that other transition-state analogues are observed to bind to the closed form of PTP1B.

The cysteine thiol was modelled as the anionic thiolate because this is the predominant form at normal physiological pH. The energy-minimized binding-site structures do not indicate a strong repulsion between thiolate and nitrate even though a gas-phase model was used and the level of theory is relatively low. Gas-phase quantum-mechanical calculations for the nitrate anion provide additional insight into the factors that stabilize the complex. Hydrogen-bond acceptors are associated with local minima in the MEP where the electric field strength (the gradient of the MEP) is zero and these minima can be seen as equivalents of the 'lone pairs' with which organic chemists are more familiar. The minimized value of the MEP ($V_{\rm min}$) has been used as a predictor of hydrogen-bond basicity for neutral compounds (Kenny, 1994) and to provide a rationale for the bioisosteric relationship between carboxylate and tetrazole anions (Kenny, 2009). Eight MEP stationary points (Fig. 4) were observed for the nitrate anion and these consisted of six equivalent minima in the plane defined by the atomic nuclei and two equivalent saddle points on the normal to this plane passing through the nitrogen nucleus. This normal to the nitrate plane represents the line of approach between thiolate and nitrate in the crystal structure. The electrostatic potential is much more negative at the minima in the plane than at the saddle points on the normal to it, suggesting that nitrate anion will be less repulsive to another anion approaching along this normal. Polarization of the nitrate by the protein can be seen as exaggerating an imbalance in its electronic distribution that is already present in the gas phase.

The relevance of MEP calculations to molecular recognition extends beyond the specific example of the nitrate anion presented in this article. These quantum-mechanical calculations show that the electrostatic fields around ions can be significantly anisotropic and that repulsions between ions of the same charge may not be as strong as they are commonly thought to be. MEP calculations suggest that it can be helpful think about charge distributions 'within' atoms as influencing molecular interactions. Another example of the use of MEP to provide insight into molecular recognition is provided by the σ-hole description of halogen bonding (Clark *et al.*, 2007).

In conclusion, we have determined a crystal structure that represents two previously uncharacterized points on the PTP1B reaction pathway and have demonstrated that quantum-mechanical calculations are consistent with the crystal structure. We have also shown how the computed MEP can provide additional insight into the nature of the interactions between nitrate anion and PTP1B.

We thank Regina Surjadi and Tam Pham for technical assistance in protein expression and purification. We also thank Paul Savage for support, the CSIRO Collaborative Crystallization Centre (http://www.csiro.au/c3) for crystallization, and the Australian Synchrotron and the beamline scientists at the MX-1 beamline for their support and technical expertise in data collection.

References

Ala, P. J., Gonneville, L., Hillman, M. C., Becker-Pasha, M., Wei, M. *et al.* (2006). *J. Biol. Chem.* **281**, 32784–32795.
Ala, P. J., Gonneville, L., Hillman, M., Becker-Pasha, M., Yue, E. W. *et al.* (2006). *J. Biol. Chem.* **281**, 38013–38021.
Asante-Appiah, E., Patel, S., Dufresne, C., Roy, P., Wang, Q., Patel, V., Friesen, R. W., Ramachandran, C., Becker, J. W., Leblanc, Y., Kennedy, B. P. & Scapin, G. (2002). *Biochemistry*, **41**, 9043–9051.
Bernstein, F. C., Koetzle, T. F., Williams, G. J., Meyer, E. F. Jr, Brice, M. D., Rodgers, J. R., Kennard, O., Shimanouchi, T. & Tasumi, M. (1977). *J. Mol. Biol.* **112**, 535–542.
Black, E. *et al.* (2005). *Bioorg. Med. Chem. Lett.* **15**, 2503–2507.
Brandão, T. A. S., Hengge, A. C. & Johnson, S. J. (2010). *J. Biol. Chem.* **285**, 15874–15883.
Chen, V. B., Arendall, W. B., Headd, J. J., Keedy, D. A., Immormino, R. M., Kapral, G. J., Murray, L. W., Richardson, J. S. & Richardson, D. C. (2010). *Acta Cryst.* D**66**, 12–21.
Clark, T., Hennemann, M., Murray, J. S. & Politzer, P. (2007). *J. Mol. Model.* **13**, 291–296.
Combs, A. P. (2010). *J. Med. Chem.* **53**, 2333–2344.
Elchebly, M., Payette, P., Michaliszyn, E., Cromlish, W., Collins, S., Loy, A. L., Normandin, D., Cheng, A., Himms-Hagen, J., Chan, C.-C., Ramachandran, C., Gresser, M. J., Tremblay, M. L. & Kennedy, B. P. (1999). *Science*, **283**, 1544–1548.
Emsley, P., Lohkamp, B., Scott, W. G. & Cowtan, K. (2010). *Acta Cryst.* D**66**, 486–501.
Engh, R. A. & Huber, R. (1991). *Acta Cryst.* A**47**, 392–400.
Fauman, E. B., Yuvaniyama, C., Schubert, H. L., Stuckey, J. A. & Saper, M. A. (1996). *J. Biol. Chem.* **271**, 18780–18788.
Frisch, M. *et al.* (2009). *Gaussian* 03, revision B04. Gaussian Inc., Wallingford, Connecticut, USA
Grimme, S., Antony, J., Schwabe, T. & Mück-Lichtenfeld, C. (2007). *Org. Biomol. Chem.* **5**, 741–758.

Han, Y., Belley, M., Bayly, C. I., Colucci, J., Dufresne, C., Giroux, A., Lau, C. K., Leblanc, Y., McKay, D., Therien, M., Wilson, M.-C., Skorey, K., Chan, C.-C., Scapin, G. & Kennedy, B. P. (2008). *Bioorg. Med. Chem. Lett.* **18**, 3200–3205.
Kabsch, W. (2010). *Acta Cryst.* D**66**, 125–132.
Karplus, P. A. & Diederichs, K. (2012). *Science*, **336**, 1030–1033.
Kenny, P. W. (1994). *J. Chem. Soc. Perkin Trans. 2*, pp. 199–202.
Kenny, P. W. (2009). *J. Chem. Inf. Model.* **49**, 1234–1244.
Lau, C. K. *et al.* (2004). *Bioorg. Med. Chem. Lett.* **14**, 1043–1048.
Liu, G., Xin, Z., Pei, Z., Hajduk, P. J., Abad-Zapatero, C., Hutchins, C. W., Zhao, H., Lubben, T. H., Ballaron, S. J., Haasch, D. L., Kaszubska, W., Rondinone, C. M., Trevillyan, J. M. & Jirousek, M. R. (2003). *J. Med. Chem.* **46**, 4232–4235.
McCoy, A. J., Grosse-Kunstleve, R. W., Adams, P. D., Winn, M. D., Storoni, L. C. & Read, R. J. (2007). *J. Appl. Cryst.* **40**, 658–674.
Murshudov, G. N., Skubák, P., Lebedev, A. A., Pannu, N. S., Steiner, R. A., Nicholls, R. A., Winn, M. D., Long, F. & Vagin, A. A. (2011). *Acta Cryst.* D**67**, 355–367.
Pannifer, A. D. B., Flint, A. J., Tonks, N. K. & Barford, D. (1998). *J. Biol. Chem.* **273**, 10454–10462.
Peters, K. G., Davis, M. G., Howard, B. W., Pokross, M., Rastogi, V., Diven, C., Greis, K. D., Eby-Wilkens, E., Maier, M., Evdokimov, A., Soper, S. & Genbauffe, F. (2003). *J. Inorg. Biochem.* **96**, 321–330.
Puius, Y. A., Zhao, Y., Sullivan, M., Lawrence, D. S., Almo, S. C. & Zhang, Z.-Y. (1997). *Proc. Natl Acad. Sci. USA*, **94**, 13420–13425.
Scapin, G. *et al.* (2003). *Biochemistry*, **42**, 11451–11459.
Szabo, A. & Ostlund, N. S. (1996). *Modern Quantum Chemistry: Introduction to Advanced Electronic Structure Theory*. Mineola: Dover Publications.
Whittier, S. K., Hengge, A. C. & Loria, J. P. (2013). *Science*, **341**, 899–903.
Winn, M. D. *et al.* (2011). *Acta Cryst.* D**67**, 235–242.
Xin, Z., Liu, G., Abad-Zapatero, C., Pei, Z., Szczepankiewicz, B. G., Li, X., Zhang, T., Hutchins, C. W., Hajduk, P. J., Ballaron, S. J., Stashko, M. A., Lubben, T. H., Trevillyan, J. M. & Jirousek, M. R. (2003). *Bioorg. Med. Chem. Lett.* **13**, 3947–3950.
Zhang, S. & Zhang, Z.-Y. (2007). *Drug Discov. Today*, **12**, 373–381.